IITB-PHY160916
MITP/16-075

Late decaying 2-component dark matter scenario as an explanation of the AMS-02 positron excess

Jatan Buch,[1,2,*] Pranjal Ralegankar,[1,†] and Vikram Rentala[1,‡]

[1]*Department of Physics, Indian Institute of Technology - Bombay, Powai, Mumbai 400076, India*
[2]*PRISMA Cluster of Excellence, 55099 Mainz, Germany and Mainz Institute for Theoretical Physics, Johannes Gutenberg-Universität Mainz, 55099 Mainz, Germany*

arXiv:1609.04821v1 [hep-ph] 15 Sep 2016

Abstract

The long standing anomaly in the positron flux as measured by the PAMELA and AMS-02 experiments could potentially be explained by dark matter annihilations. This scenario typically requires a large "boost factor" to be consistent with a thermal relic dark matter candidate produced via freeze-out. However, such an explanation has been considered to be disfavored by constraints from CMB observations on energy deposition during the recombination epoch. In this work, we construct a scenario for late-decaying two-component dark matter (LD2DM) with almost degenerate dark matter species. We show that such a scenario can explain the observed AMS-02 positron flux through an annihilation of the lighter dark matter species, while avoiding CMB constraints. The observed relic density can be correctly reproduced as well, with simple s-wave annihilation cross-sections. We demonstrate that the scenario is robust, subject to constraints from structure formation and CMB constraints on late-time energy depositions during the cosmic "dark ages". We briefly explore possible cosmological and particle physics signatures in a toy model that realizes this scenario.

PACS numbers: 95.35.+d,96.50.S-,98.80.Cq,95.85.Ry

*Electronic address: jatan_buch@brown.edu
†Electronic address: pranjal.238@gmail.com
‡Electronic address: rentala@phy.iitb.ac.in

I. INTRODUCTION AND MOTIVATION

The cosmic ray positron flux measured at Earth shows an excess with respect to the secondary positrons, produced by cosmic rays spallations on the interstellar medium (ISM), at energies above 10 GeV. This was confirmed through a measurement of a rising positron fraction up to 100 GeV by the PAMELA [1] and FERMI satellites [2]. Interestingly, there has been no observed excess in the corresponding cosmic antiproton flux [3, 4]. Recently, high precision data up to 500 GeV for the positron fraction (defined as the ratio of the e^+ to $(e^+ + e^-)$ flux) has been released by the AMS-02 detector onboard the International Space Station (ISS) [5]. One of the most intriguing features of the AMS-02 data is that the positron fraction does not appear to be increasing for energies above ~ 200 GeV [5].

Quantifying the positron excess from the positron fraction typically requires a detailed modelling of the background secondary positrons as well as the primary electron flux. For the first time, the AMS-02 collaboration has released data for the electron and positron fluxes separately [6], along with the updated $(e^+ + e^-)$ flux [7] and positron fraction data. This is significant since it allows for an analysis of the positron excess without modelling the primary electron spectrum [8], or using data from another experiment [9]. Regardless of the background uncertainties, it is beyond reasonable doubt that there is an excess of a primary positron component beyond the secondary astrophysical background from spallations [10], although there is no consensus yet on our understanding of other astrophysical sources of positrons.

Indeed, purely astrophysical interpretations for a new primary positron component have been proposed, through three-dimensional modelling of cosmic ray sources [11], or a population of pulsars localized near the Earth [12]. Although the pulsar interpretation provides a good fit to the data for reasonable choices of spectral parameters and spatial distributions (see for example [13] or [14] for a recent appraisal), we shall not discuss it further and refer the interested reader to the literature [15–17]. Instead, we argue the case for an annihilating dark matter (DM) interpretation of the positron excess.

Weakly Interacting Massive Particles (WIMPs) are among the most popular DM candidates, as they can arise 'naturally' within models extending the Standard Model (SM) beyond the electroweak symmetry breaking (EWSB) scale. The typical scenario for production of WIMPs in the early universe is via the freeze-out mechanism [18]. The velocity-averaged s-wave annihilation cross-section (only cross-section henceforth) to achieve a DM thermal relic density consistent with the current value $\Omega_{\rm DM}h^2 = 0.1193 \pm 0.0014$ [19], is computed to be $\langle\sigma v\rangle_{\rm TR} = 2.2 \times 10^{-26}\,{\rm cm}^3/{\rm s}$ [20], which is coincidentally typical for a $\sim$ TeV scale dark matter particle with SM-like weak couplings. This coincidence has been dubbed the "WIMP miracle".

Indirect detection signals of WIMP annihilation provide a complementary probe to searches for dark matter at colliders and direct detection experiments. An excess in the positron flux has long been touted as a 'smoking gun' signature for WIMP dark matter annihilations in the Milky Way galactic halo [21]. An analysis of the energy range of the positron excess as well as the observed spectral shape and normalization allows for a good fit to a $\sim$ TeV scale dark matter particle with a velocity-averaged cross-section $\langle\sigma v\rangle \sim 10^{-24}$ - $10^{-21}\,{\rm cm}^3/{\rm s}$ annihilating predominantly into a W^+W^- pair, or into SM leptons [22]. Note that this cross-section is $\sim 10^2$ - 10^5 times larger than the standard freeze-out cross-section.

There are two ways to resolve this discrepancy within the standard WIMP paradigm. The first way is to assume a velocity dependent Sommerfeld enhancement factor to the cross-section. The approximately inverse dependence of this factor on velocity leaves the early universe cross-section (during the epoch of freeze-out) essentially unchanged but leads to a large enhancement in the present day annihilation cross-section due to the low DM velocities ($v \sim 10^{-3}c$) that are present in our galaxy today. It has been shown that DM interactions mediated by SM bosons [23, 24], or by a new light mediator [25, 26] can give rise to this kind of enhancement. The second approach is to consider astrophysical "boost factors" to the annihilation flux, where overdense regions in the local galactic halo may enhance the DM annihilation rate [27] over the canonical assumption of a smooth dark matter distribution. However in this case, the boost factors have been found to be typically of $\mathcal{O}(10)$ [28], which is an insufficient enhancement.

The annihilating DM interpretation of the positron excess is subject to two types of constraints – from present day astrophysical observations and from early universe constraints arising from cosmic microwave background (CMB) observations.

Astrophysical constraints arise from multi-messenger observations of data from gamma-ray detectors and radio telescopes [29–34]. Observations of diffuse gamma rays, gamma rays from dwarf galaxies and radio observations give rise to constraints on annihilating dark matter scenarios. Uncertainty in the intervening astrophysics: DM density profiles [35], galactic magnetic field modelling [36, 37] and propagation parameters [38], weakens most of these indirect detection constraints allowing some room for a DM interpretation of the positron excess.

However, early universe constraints from observations of CMB temperature and polarization anisotropy spectra reflecting conditions near the epoch of recombination [39, 40] provide far more robust and stringent constraints. Naive s-wave DM cross-sections that explain the positron excess are strongly excluded by these CMB observations. For models with Sommerfeld enhancement, the DM velocity near the epoch of recombination ($v \approx 10^{-8}\, c$) implies that the cross-section is saturated to its maximum value – greatly exceeding the constraint set by the CMB observations.

Thus, in light of the CMB constraints, an annihilating DM interpretation of the positron excess has fallen out of favor. In this work we examine the assumptions behind the CMB constraints and we show that these constraints can be relaxed in the event of a non-thermal production mechanism for the dark matter particle. We propose a late decaying two-component DM (LD2DM) scenario where the dark sector consists of two semi-degenerate dark sector particles which we denote as χ_1 (heavier) and χ_2 (lighter)[1]. Both species are assumed to have simple s-wave annihilation cross-sections. The lighter dark matter particle χ_2 is the stable DM candidate that populates the universe today and annihilates with a large annihilation cross-section to SM particles in order to explain the observed positron excess. The large annihilation cross-section of χ_2 ensures that it was underproduced in the early universe. The heavy species χ_1 is assumed to have the required thermal freeze-out cross-section with which it annihilates to a radiation bath. Thus, in the early universe χ_1 plays the role of dark matter with the correct relic density. The heavy species χ_1 decays on a cosmological

[1] Such a class of models has been proposed in the literature [41–45] primarily to address the departure, on small scales, of Cold Dark Matter (CDM) simulations from observations [46–52].

timescale through the process,

$$\chi_1 \to \chi_2 + n\phi.$$

Here, $n\phi$ in general stands for one or more light dark sector particles (dark radiation). The late decays of χ_1 convert it into χ_2 (which makes up the present day dark matter) on cosmological timescales. The late production of χ_2 ensures that its annihilations to SM particles do not affect the CMB during the epoch of recombination.

The rest of the paper is organised thus: In Sec. II we revisit the positron flux data from AMS-02 and find the best fit dark matter annihilation parameters needed to explain the positron excess. We also compare these best fit parameters with constraints from astrophysical and cosmological observations. In Sec. III we discuss the tension between the standard WIMP paradigm explanation of the positron excess and (1) demanding the correct relic density (2) CMB temperature and polarization anisotropy constraints on DM annihilation in the early universe. In Sec. IV we motivate and present the basic LD2DM scenario as a possible reconciliation of this conflict, while explaining the observed positron excess. In Sec. IV A we discuss how this reconciliation is achieved and in Sec. IV B we examine constraints that arise on the basic LD2DM scenario, from late time energy depositions (and their effect on the CMB) and from observations of small scale structure. In Sec. V we propose a toy particle physics model and briefly explore a few phenomenological implications. We highlight a few general cosmological features of the LD2DM scenario in Sec. VI. Finally, we conclude with an overview of the key results from the paper in Sec. VII. Details about the properties and parameters used for solving the propagation equation relevant for Sec. II can be found in the Appendix.

II. DARK MATTER AND THE POSITRON EXCESS

Over the years the cosmic ray (CR) spectra have been measured, to varying degrees of precision, by different experiments. The data for the positron fraction has been released by PAMELA [1], FERMI [2], and most recently by AMS-02 [5, 53]; for the total electron and positron ($e^+ + e^-$) spectrum by FERMI [54] and AMS-02 [7]; and for the antiproton spectrum by PAMELA [3] and AMS-02 [4]. The most intriguing feature that emerges from the data is that the positron fraction exhibits a steep increase at energies greater than $\sim$ 10 GeV over the secondary background of positrons expected from CR spallations on the interstellar medium (ISM), whereas no significant excess is observed for antiprotons. Moreover, measurements of the individual electron (e^-) flux by PAMELA [55] and FERMI prove that the rising positron fraction is indeed due to an excess in the positron (e^+) flux, rather than a decline in the e^- flux. Together, this points towards the presence of a new primary component of positrons, of an astrophysical origin [11–17] or a more exotic origin like DM annihilations.

In this work, we will focus only on the DM interpretation of the positron excess. An absence of a complementary excess, within uncertainties, in the antiproton spectrum [56] indicates that DM annihilation channels with purely leptonic final state are preferred. As noted by [22], a $\sim$ TeV scale DM particle annihilating, directly or through an intermediate state, to SM leptons with a cross-section $\mathcal{O}(1000)$ times larger than the thermal relic value gives a reasonably good fit to the positron excess data.

A recent release of high-precision measurements exclusively for the e^+ flux by AMS-02 (see

black data points in Fig. 1) allows us to fit the positron flux from DM annihilations directly to the data, without any modelling of the electron spectrum [8] and avoiding the introduction of systematic errors from using $(e^+ + e^-)$ data from the same (or other) experiments [9, 13, 14]. This motivates another look at the DM interpretation of the positron excess. In Sec. II A, we will revisit the dark matter interpretation and recompute the best fit dark matter cross-section and mass parameters. In Sec. II B, we will examine astrophysical and cosmological constraints on these parameters.

A. Revisiting the DM interpretation of the positron excess

In order to interpret the positron spectrum, we first model the sources of (secondary) positrons from astrophysics, then introduce a primary component from DM annihilations to explain the excess.

We compute the astrophysical background, or the secondary positron spectrum, produced by nuclei in high-energy cosmic rays scattering off of the atoms of the interstellar medium by using the Dragon code [57], for the choice of nuclear CR source parameters described in Appendix A 2. As discussed in [58], we also include an enhancement factor, c_{e^+}, for the secondary positrons to fit the low energy positron flux data. This factor can be viewed as a quantifier of the uncertainties in the effective proton-proton cross-section due to the presence of heavier nuclei in cosmic rays and in the ISM [59].

The primary component of positron flux is assumed to be comprised of positrons produced from DM annihilations in the Milky Way halo. Due to a lack of complementary excess in the antiproton spectrum, we will consider DM annihilations in only four channels with leptonic final states: $\mu^+\mu^-$, $\tau^+\tau^-$, 4μ, 4τ. The spectra of positrons obtained per annihilation can be obtained from the results in PPPC4DMID[2] [60, 61]. The spatial distribution of DM in the galactic halo is assumed to be described by a Navarro-Frenk-White (NFW) density profile [62] which is parameterized by a spherically symmetric distribution function,

$$\rho(r) = \frac{\rho_s}{(r/r_s)(1 + r/r_s)^2}. \tag{1}$$

Here r is the distance from the galactic center, $\rho_s = 0.26$ GeV cm^{-3} and $r_s = 20$ kpc such that the DM density at Earth is normalized to $\rho_\odot = 0.3$ GeV cm^{-3} [63]. The DM velocity-averaged annihilation cross-section ($\langle\sigma v\rangle$) and mass (m_χ), which determine the normalization and position of the peak of the positron flux respectively, are treated as free parameters which we will fit for when comparing the total predicted positron flux to the data.

Once we model the sources of positrons, we need to consider the propagation of the positrons from the sources to the earth. Positrons produced in DM annihilations, or from a secondary astrophysical process, propagate through the turbulent galactic magnetic field (GMF) and get deflected by random inhomogeneities, referred to as Alfv́en waves [64, 65]. While diffusing from their sources to the Earth, the positrons lose energy through several processes such as spiralling through the galactic magnetic field emitting synchrotron

[2] http://www.marcocirelli.net/PPPC4DMID.html. We note that the mediators in the PPPC4DMID codes for the 4μ and 4τ channels are assumed to be light compared to the DM mass.

radiation, through inverse Compton scattering (ICS) on the CMB and ambient starlight, bremsstrahlung, possible reacceleration or convection, and other sub-dominant processes. The propagation of positrons can be modelled by a diffusion equation with the appropriate choices of propagation profiles and GMF models. A propagation profile is defined by a set of parameters that occurs in the diffusion equation whose values are inferred from fits to data of secondary-to-primary ratios of nuclei in cosmic ray spectra (refer Appendix A 1 for a detailed discussion). It is important to note that current precision in the data of secondary-to-primary ratios cannot help us distinguish between the degeneracies in different propagation profiles. However, the exquisite (albeit preliminary) B/C ratio data presented by AMS-02 [66] indicates that we are entering a new era of precision astrophysics [38], and consequently the current propagation models (for example: the MIN-MED-MAX profiles [67, 68] used in [14]) must be updated in accordance with the data. In our analysis, we take a preliminary step in that direction by adopting two propagation profiles that incorporate the new AMS-02 data: MOD A [58] and MOD B [69], and a 'realistic' model for the GMF [70] (Appendix A 3). We implement these in the Dragon code, which we use to solve the propagation equation numerically. The total local interstellar positron flux (LIF) after propagation, denoted as $\Phi_{e^+}^{\rm tot,LIF}(E)$ (indicated by the blue dot-dashed line in Fig. 1) is given by a sum of the DM contribution and the contribution from secondaries,

$$\Phi_{e^+}^{\rm tot,\ LIF}(E) = \Phi_{e^+}^{\rm DM}(E) + c_{e^+}\Phi_{e^+}^{\rm sec}(E). \tag{2}$$

In order to obtain the positron flux measured at Earth however, solar modulation effects must also be considered. We account for this using the force-field approximation [71] and fix the value of the Fisk potential to $\phi_{\rm F} = 600\,{\rm MV}$ [72]. Thus, for each annihilation channel for the DM, for a given cross-section and mass, we can compute the solar modulated flux of positrons expected at Earth as,

$$\Phi_{e^+}^{\rm tot,\ modulated}(E) = \frac{E^2}{(E+\phi_{\rm F})^2}\Phi_{e^+}^{\rm tot,\ LIF}(E+\phi_{\rm F}). \tag{3}$$

We then proceed to fit the dark matter cross-section and mass by comparing the positron flux computed in Eq. (3), $\Phi_{e^+}^{\rm tot,\ modulated}$, to the flux observed by AMS-02, $\Phi_{e^+}^{\rm obs}$. We choose to use only the high precision e^+ flux data released by AMS-02 (see black data points in Fig. 1), rather than the positron fraction data for comparison of our theoretical predictions with experiment. This choice of data set allows us to extract the expected DM parameters without any modelling of the electron spectrum [8] and also avoids the introduction of systematic errors from using $(e^+ + e^-)$ data from the same (or other) experiments [9, 13, 14].

We calculate the χ^2 value, defined as

$$\chi^2 = \sum_i \frac{\left(\Phi_{e^+,i}^{\rm obs} - \Phi_{e^+,i}^{\rm tot,\ modulated}\right)^2}{\sigma_i^2}, \tag{4}$$

where the sum in i runs over 49 energy bins of the AMS-02 data and we take σ_i to be the value of statistical and systematic errors added in quadrature for each bin. Finally, we derive the reduced-χ^2 ($\chi^2_{\rm dof}$) by dividing the χ^2 by the degrees of freedom, *i.e.* the number of data-points minus the number of free parameters of the fit. Initially, we do a crude scan over three parameters m_χ, $\langle\sigma v\rangle$ and c_{e^+}. We use this to fix the value of c_{e^+} and then do a more

refined scan over the m_χ and $\langle\sigma v\rangle$ values. The χ^2-minimization is performed separately for the MODA and MODB propagation profiles.

The best-fit values for c_{e^+}, m_χ and $\langle\sigma v\rangle$, based on the minimization of χ^2, have been tabulated in Tab. 1 for all four leptonic final states that we consider and for both propagation profiles. Using the values in this table, in Fig. 1 we plot the primary positron spectrum from DM annihilations in the 4μ and 4τ annihilation channels, the total LIF calculated in Eq. (2), and the best fit prediction of the total positron flux at Earth after including the solar modulation effects.

TABLE 1: Best fit values for DM parameters in case of leptophilic annihilation channels. The $\chi^2_{\rm dof}$ values are computed as elaborated in the text.

Propagation Profile	Channel	m_χ [GeV]	$\langle\sigma v\rangle$ [cm^3/s]	c_{e^+}	$\chi^2_{\rm dof}$
MODA	$\mu^+\mu^-$	340	2.42×10^{-24}	1.80	2.99
	$\tau^+\tau^-$	800	1.73×10^{-23}	1.63	0.68
	$Z'Z'\to4\mu$	570	4.57×10^{-24}	1.72	1.49
	$Z'Z'\to4\tau$	1700	3.63×10^{-23}	1.70	0.72
MODB	$\mu^+\mu^-$	350	2.42×10^{-24}	2.20	3.11
	$\tau^+\tau^-$	880	1.77×10^{-23}	2.10	0.76
	$Z'Z'\to4\mu$	570	2.10×10^{-24}	2.10	1.66
	$Z'Z'\to4\tau$	1760	1.70×10^{-23}	2.10	0.80

Fig. 1 indicates that the low energy bins receive a contribution mostly from the secondary background, while the peaked primary positron spectra from DM annihilations drives the fit in the high energy bins. Thus, the predicted behavior of a falling positron spectra above 500 GeV is one of the key features that will help in distinguishing between a DM and pulsar interpretation of the positron excess [73].

Our best fit values for the enhancement factor to the secondary background, c_{e^+}, are in close agreement with [58] for the MODA profile. The MODB profile provides a good fit to the positron flux data, however the best fit value of c_{e^+} is greater than 2 for all DM annihilation channels, exceeding the maximum expected enhancement for the effective proton-proton cross-section as per [59]. Thus, we only consider the MODA propagation profile henceforth.

With reference to the MODA profile, we observe from Tab. 1 that the 2μ annihilation channel is disfavored due to its poor fit quality, where as the 2τ and 4τ annihilation channels give very good fits to the data due to the softer e^+ spectrum obtained from these finals states. We also note that the 4μ channel provides a reasonable fit to the data as well.

Similar analysis with the latest AMS-02 data set have been carried out in [14, 58, 69] and our results are in general agreement with theirs. In particular, as we work with the positron flux data with no modelling of the primary electron spectrum, we expect our best fit region in the m_χ and $\langle\sigma v\rangle$ plane to be similar to the region obtained in [14][3], and indeed this is the

[3] The authors of [14] first obtain the total predicted positron flux by adding a primary DM (or pulsar)

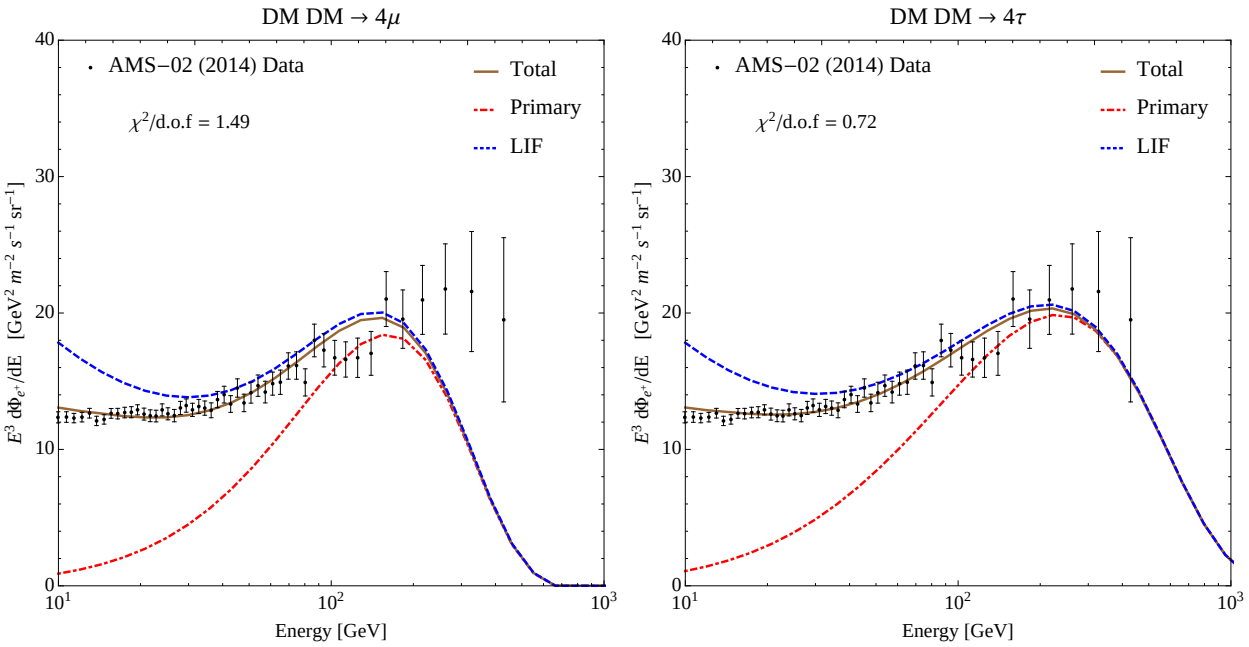

FIG. 1: The positron flux as a function of positron energy for the 4μ channel (left) and 4τ channel (right) corresponding to the best-fit values of $\langle\sigma v\rangle$ and m_χ for the MODA profile. The $\chi^2_{\rm dof}$ for each channel is also indicated in the plot.

case. We highlight two differences in our results however: (1) since we include a complete description of the energy losses and a new, improved model for GMF in the Dragon code, this gives us an increased total positron flux, pushing the best fit point towards slightly lower cross-sections, (2) there is an overall improvement in the quality of our fits.

B. Constraints on dark matter interpretations of the positron excess

The annihilating DM interpretation of the positron excess obtained in the previous subsection is subject to astrophysical and cosmological constraints. We consider each of these in turn.

Astrophysical constraints: The annihilation products of the DM should cascade to produce gamma rays as well as undergo acceleration in the galactic magnetic field to produce synchrotron radiation in radio frequencies. Therefore, the annihilating DM interpretation is subject to constraints from multi-messenger analysis from radio and gamma ray spectral data. The radio constraints are subject to large uncertainties inherent in modelling of the GMF (see [30] for a recent update), so we only focus on constraints that arise from measurement of the gamma ray spectrum. There are two types of constraints arising from (1) measurements of the gamma ray flux from Milky Way dwarf spheroidal galaxies (dSphs) (by Fermi-LAT [33, 34], VERITAS [74] and HESS [75]) and (2) from diffuse gamma ray measure-

positron component over the astrophysical background, then use the preliminary $(e^+ + e^-)$ spectra released by AMS-02 to compute the predicted positron fraction, which they finally fit to the AMS-02 positron fraction data.

ments. The constraints arising from gamma ray measurements are obviously annihilation channel dependent. While the 2τ channel provides the best fit to the positron flux data, it is strongly ruled out by gamma ray constraints from dSphs, we will therefore only consider the 4μ and 4τ annihilation channels in what follows.

Our computation of the best fit 1σ and 2σ contours for the DM annihilation cross-section and mass (based on our fits to the AMS-02 positron flux) for the 4μ and 4τ channels are shown in Fig. 2. In the same figure, we also show the 2σ upper confidence limit of the DM annihilation cross-section in these channels, using Fermi-LAT data for the stacked dSph galaxy gamma ray flux adapted from [76, 77][4]. We observe that the 4μ annihilation cross-section needed to explain the positron excess is safe from the dSph bound and is thus a viable annihilation channel for the DM. However, the exclusion bounds obtained by these authors appear to rule out the best fit value of the DM cross-section needed to explain the positron excess in the 4τ channel. We note that these naive bounds are not robust. Upon including uncertainties: choice of DM density profiles, non-sphericity etc. for the dSphs, the gamma ray constraints may weaken by a factor $\sim$ few depending on the modelling of the DM density profile [78–80], allowing room for even the 4τ annihilation channel.

We also include in Fig. 2 the 3σ exclusion curve for the 4μ channel from the Fermi *diffuse gamma ray measurements* [81], which only has a mild dependence on the Milky Way DM density profile and is thus more robust than the dSph bound. This bound is conservative, since it attempts to attribute the entire observed diffuse gamma ray flux to DM annihilations without modelling astrophysical sources. We note from the figure that the cross-section needed to explain the positron excess in the 4μ channel is safe from this diffuse gamma ray bound[5].

Cosmological constraints: The most robust and stringent constraints on DM annihilating with large cross-sections comes from the effects of energy deposition into the thermal plasma in the early universe and the consequent effect on the CMB temperature and polarization anisotropies. DM annihilations around the epoch of recombination increase the residual ionization compared to the cosmological ionization history expected in standard ΛCDM scenarios with non-annihilating DM. For the typical cross-sections under consideration, the increased ionization fraction leaves the peak of the visibility function unchanged, which signifies that the redshift of the last scattering surface (LSS) remains undisturbed. However, the LSS undergoes a broadening [39, 40], which leaves an imprint on both temperature and polarization spectra of the CMB. The temperature fluctuations on scales smaller than the thickness of the LSS (measured using conformal time) are suppressed, causing a relative attenuation of the power spectrum on these scales, as compared to the standard scenario with non-annihilating DM. This effect alone does not lead to strong bounds on the

[4] These bounds assume that the DM annihilation is mediated by a mediator particle, whose mass is much lighter than the dark matter mass. In the case of the 4μ annihilation channel [77], as pointed out by [76], radiative corrections must also be included to obtain a competitive constraint, whereas considering only final state radiation (FSR) suffices to set a bound for the 4τ channel.

[5] We note that the bound in [81] has been computed using the preliminary Fermi diffuse gamma ray measurements, and the authors have not computed a similar bound for the 4τ channel. An updated analysis accounting for the foreground astrophysical diffuse emission has been performed in [32], however this work does not examine the 4μ and 4τ channels.

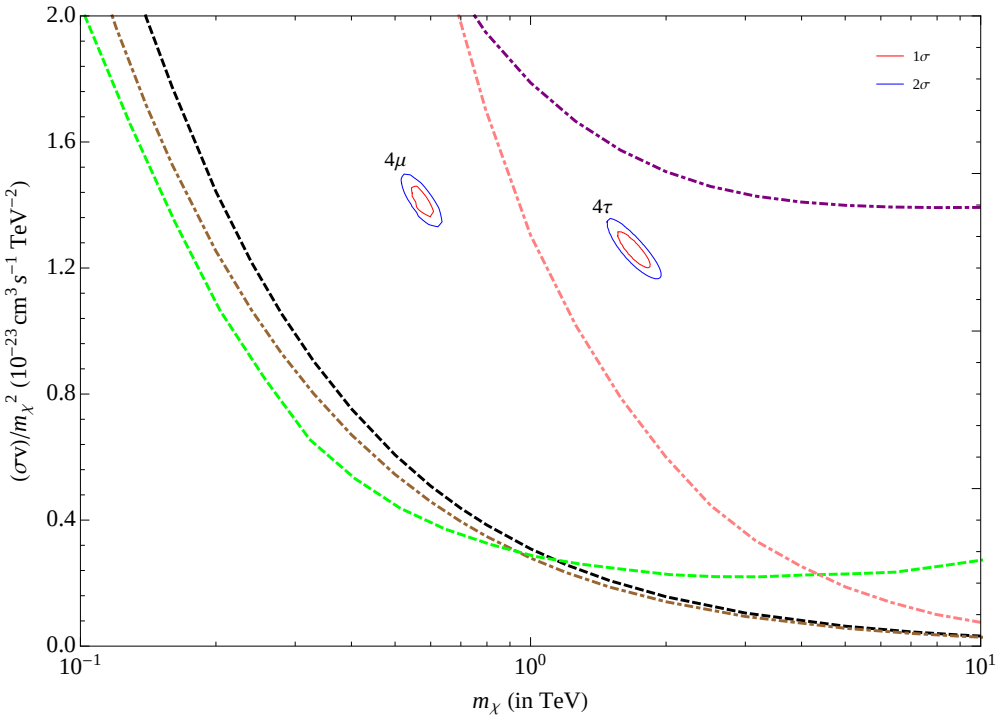

FIG. 2: The 1σ and 2σ contours of the best-fit region for a DM explanation of the positron excess are indicated in red and blue respectively for the 4μ and 4τ annihilation channels. Astrophysical constraints from FERMI measurements of gamma rays in dwarf spheroidal galaxies (dSphs) for the 4μ (purple, dot-dashed), 4τ (green, dashed) channels adopted from [76, 77], and diffuse gamma constraints for the 4μ (pink, dot-dashed) channel [81] are also shown. We have also plotted CMB recombination-era constraints computed using [82, 83] for the 4μ (brown, dot-dashed) and 4τ (black, dashed) channels. NOTE: The CMB constraints depend on the assumed cosmological history and do not apply in the LD2DM scenario as discussed in the text.

DM parameters since it is almost completely degenerate with a change in the slope and amplitude of the primordial power spectrum. On the other hand, the effects of broadening of the LSS on polarization spectrum are more distinct. Other than an attenuation effect on small scales, there is also an increase in the amplitude together with a slight shift in the peaks of the E-mode polarization spectrum [84]. This allows us to constrain the DM mass and annihilation cross-section. In Fig. 2, we plot the latest constraints on the DM annihilation cross-sections in the 4μ and 4τ channels following CMB anisotropy measurements by Planck [19], using publicly available recipes [82, 83]. We see that the CMB constraints are severe and strongly rule out the best-fit DM annihilation masses and cross-sections needed to explain the observed positron excess. We point out here that these CMB bounds are derived under two assumptions (1) that the annihilating DM had a comoving number density (n) from around the epoch of recombination till today that varied with redshift (z) as $n \propto (1+z)^3$, i.e. there were no number changing dark matter processes post recombination. This assumption is typical of most DM cosmological histories, including the scenario of WIMPs produced via freeze-out. (2) that the annihilation cross-section $\langle \sigma v \rangle$ is velocity independent (i.e. s-wave scattering cross-section).

We summarize this section by noting that the AMS-02 positron excess can *prima facie* be explained by dark matter annihilating to 4μ or 4τ final states, with cross-sections and masses as given in Tab. 1. Astrophysical constraints arising from the diffuse gamma ray background and gamma rays from dwarf galaxies cannot rule out these annihilation channels, due to the large astrophysical uncertainties intrinsic to modelling the predicted gamma ray flux. However, under some simple assumptions, CMB constraints prove to be extremely stringent and strongly rule out the best fit cross-sections and masses that we have determined, putting a DM interpretation of the AMS-02 positron excess in jeopardy.

III. BEYOND THE THERMAL WIMP PARADIGM

As we have seen in the previous section, there are stringent constraints from CMB observations on a dark matter interpretation of the positron excess. We point out though, that the contours in Fig. 2 have been plotted under the assumptions that there were no number changing DM interactions in the era leading up to recombination till today and that the value of $\langle \sigma v \rangle$ for annihilating DM at recombination is equal to the one that explains the positron excess today. These assumptions implicitly constrain the cosmological evolution of the DM particle(s).

For example, within a standard WIMP DM scenario, the DM is a thermal relic that undergoes freeze-out [18] with a cross-section given by $2.2 \times 10^{-26}\,\mathrm{cm}^3/\mathrm{s}$ [20]. However, the cross-sections required to explain the AMS-02 positron excess are much larger than this value and invoking these cross-sections would give rise to too low a relic density in the early universe if we assume the standard freeze-out paradigm. One alternative is to posit an astrophysical boost factor from dark matter clumping on small scales [27] in the galactic halo. This would enhance the annihilation rate in the present universe as compared to the standard expectation from an NFW (or other standard halo) dark matter profile. This explanation is ruled out as the large boost factors $\mathcal{O}(1000)$ needed to explain the AMS-02 positron signal are disfavored by numerical simulations of our galaxy [28]. Another frequently discussed boost factor is the mechanism of Sommerfeld enhancement [23–26], where cross-sections are enhanced at low velocities. The velocity in galactic halos today is $10^{-3}\,c$, where c is the speed of light, as compared to $0.1\,c$ at the time of freeze-out in the early universe. This implies that the DM freezes-out with the thermal cross-section, with the correct relic abundance in the early universe, and achieves the larger cross-section necessary to explain the AMS-02 positron excess today. However, a Sommerfeld enhancement of the annihilation cross-section would lead to even more severe bounds from CMB observations since the typical WIMP velocity would be $10^{-8}\,c$ near the surface of last scattering, thereby saturating the Sommerfeld enhancement factor.

We summarize the cosmological constraints by noting here a very important point relevant to our current work: *If an s-wave or Sommerfeld enhanced annihilating dark matter species exists before the epoch of recombination, the large annihilation cross-section needed to explain the* AMS-02 *positron excess is ruled out by CMB observations.* This bound is independent of the production mechanism of the DM (see [85] for a recent review of non-thermal production mechanisms). In the next section, we propose a scenario that is consistent with the large annihilation cross-sections needed to explain the positron excess today, CMB observations, and the observed relic abundance.

IV. LATE DECAYING TWO COMPONENT DARK MATTER (LD2DM) SCENARIO

In order to explain the AMS-02 positron excess via dark matter annihilations while still being consistent with CMB constraints arising from energy deposition during the epoch of recombination, we adopt an alternate production mechanism scenario for DM which we refer to as late-decaying two-component dark matter (LD2DM). Our framework consists of two dark matter particles, χ_1 and χ_2, characterized by the decay of the heavier particle (χ_1) into the lighter particle (χ_2) on cosmological timescales through the process: $\chi_1 \to \chi_2 + n\phi$, where $n\phi$ schematically stands for any number of light dark sector particles (dark radiation). The decay occurs such that χ_2 is the stable DM that populates the universe today while χ_1 is the one populating the universe during the time of recombination. Hence, by simply attributing the large annihilation cross-section required to explain the positron excess to χ_2 and a significantly smaller one to χ_1, we are able to evade the stringent constraints set by CMB and simultaneously explain the positron excess.

This basic scenario can be described by five essential parameters, viz. the masses of χ_1 and χ_2 denoted by m_1 and m_2 respectively, the annihilation cross-sections of χ_1 and χ_2 denoted by $\langle\sigma_1 v_1\rangle$ and $\langle\sigma_2 v_2\rangle$ respectively, and finally the decay lifetime of χ_1 denoted by Γ^{-1}. In this section we shall see how each of these parameters are determined or constrained.

Since it is the annihilation of χ_2 particles in the galactic halo that gives rise to the observed AMS-02 positron excess, we assign it the mass and annihilation cross-section as laid out in Tab. 1. We consider separately the scenarios where χ_2 annihilates only to 4μ or only to 4τ. As a benchmark, we take the values $m_2 = 570$ GeV, $\langle\sigma_2 v_2\rangle = 4.57 \times 10^{-24}$ cm^3/s for the 4μ annihilation channel and $m_2 = 1700$ GeV, $\langle\sigma_2 v_2\rangle = 3.63 \times 10^{-23}$ cm^3/s for the 4τ annihilation channel.

The large annihilation cross-section of χ_2 would lead to a low abundance for this species in the early universe. We therefore assume that χ_1 has a thermal annihilation cross-section $\langle\sigma_1 v_1\rangle = 2.2 \times 10^{-26}\,\text{cm}^3/\text{s}$, so that it undergoes freeze-out and would in principle yield the correct dark matter relic density in the early universe. At this level of discussion, we can assume that χ_1 annihilates to either dark radiation or SM species. The thermal relic cross-section of this species is small enough to satisfy the constraints set on energy depositions during recombination for several SM annihilation channels. In Sec. IV A we will examine the evolution of the abundances of both species and demonstrate that the abundance of dark matter (χ_2) in the late universe is correctly reproduced.

Thus, considerations of the AMS-02 positron signal and the relic density fix the annihilation cross-sections of both species and the mass m_2. The two crucial parameters which are left undetermined are the lifetime Γ^{-1} and the mass m_1 of the heavy species. In Sec. IV B we derive the constraints on these two parameters from cosmology. We will see that bounds on the lifetime of χ_1 arise from considerations of CMB constraints on energy deposition during the recombination epoch as well as *late time energy deposition* in the cosmic "dark ages". Together these constrain $\Gamma^{-1} \gtrsim 10^{13}$ s for the 4μ (or 4τ) annihilation channel. We will also see that constraints arising from structure formation limit the typical kick velocity received by daughter particles after decay of the mother particle, and hence lead to a limit on the mass difference between χ_1 and χ_2, $\Delta m \equiv m_1 - m_2 \lesssim 0.1$ GeV.

A. Estimating the cosmological abundances of χ_1 and χ_2

We will first estimate the abundances of the number densities n_i of each dark matter particle (χ_1 and χ_2) at time t, by numerically solving the coupled Boltzmann equations:

$$\begin{aligned}\frac{dn_1}{dt} + 3Hn_1 &= -\langle\sigma_1 v_1\rangle\left({n_1}^2 - n_{1\mathrm{eq}}^2\right) - \Gamma n_1,\\ \frac{dn_2}{dt} + 3Hn_2 &= -\langle\sigma_2 v_2\rangle\left({n_2}^2 - n_{2\mathrm{eq}}^2\right) + \Gamma n_1,\end{aligned} \tag{5}$$

where $n_{i\mathrm{eq}}$, $\langle\sigma_i v_i\rangle$ ($i = 1, 2$) are the equilibrium number densities and annihilation cross-sections for each species and H is the Hubble parameter. Further, following the recipe in [18], we track the number density in a comoving volume by defining $Y_i(x) = n_i(x)/s(x)$ where $s(x)$ is the entropy density and $x = m_1/T$ is a "clock". We will use the same mass $m \equiv m_1 \simeq m_2 = 570$ GeV (1700 GeV) for the annihilation channel of 4μ (4τ) because as we shall see, structure formation constraints force them to be almost degenerate.

After these substitutions Eq. (5) takes the form,

$$\begin{aligned}\frac{x}{Y_{1\mathrm{eq}}}\frac{dY_1}{dx} &= -\left(\frac{n_{1\mathrm{eq}}\langle\sigma_1 v_1\rangle}{H(x)}\right)\left[\left(\frac{Y_1}{Y_{1\mathrm{eq}}}\right)^2 - 1\right] - \frac{\Gamma}{H(x)}\frac{Y_1}{Y_{1\mathrm{eq}}},\\ \frac{x}{Y_{2\mathrm{eq}}}\frac{dY_2}{dx} &= -\left(\frac{n_{2\mathrm{eq}}\langle\sigma_2 v_2\rangle}{H(x)}\right)\left[\left(\frac{Y_2}{Y_{2\mathrm{eq}}}\right)^2 - 1\right] + \frac{\Gamma}{H(x)}\frac{Y_1}{Y_{2\mathrm{eq}}}.\end{aligned} \tag{6}$$

We solve Eq. (6) assuming simple s-wave annihilation cross-sections $\langle\sigma_1 v_1\rangle = 2.2 \times 10^{-26}$ cm^3 s^{-1} and $\langle\sigma_2 v_2\rangle = 4.57 \times 10^{-24}$ cm^3 s^{-1} (3.63×10^{-23} cm^3 s^{-1}) for annihilation of χ_2 to 4μ (4τ). The evolution of the comoving number density in the matter dominated era for a decay lifetime $\Gamma^{-1} \sim 0.1\,\mathrm{Gyr}$ is plotted in Fig. 3. At relatively early times χ_1 and χ_2 are at their would-be freeze-out abundances which are achieved at a temperature $T \sim m/25$, well before recombination. The late decay converts χ_1 into χ_2 species, depleting the abundance of χ_1.

We can now anticipate how this scenario solves the problems outlined in section III when trying to reconcile the large DM annihilation cross-section required to explain the positron excess with the naive constraints from CMB observations. The large annihilation cross-section of χ_2 ensures that it has a low abundance in the early universe. This suppressed abundance of χ_2 in the early universe prevents its annihilation products from depositing a significant amount of energy into the thermal plasma during the recombination era. χ_2 eventually attains the correct relic density (and thus forms almost all of the present day dark matter) through the decay of χ_1. Thus, CMB constraints from the broadening of the surface of last scattering should not apply as long as $\Gamma^{-1} \gtrsim 380,000$ years. One might worry that the CMB observations would constrain potential annihilations of χ_1 to SM particles, however the cross-section $\langle\sigma_1 v_1\rangle$ is low enough to evade the CMB bounds. In the next subsection we will examine the CMB constraints on the annihilation of χ_2 in detail.

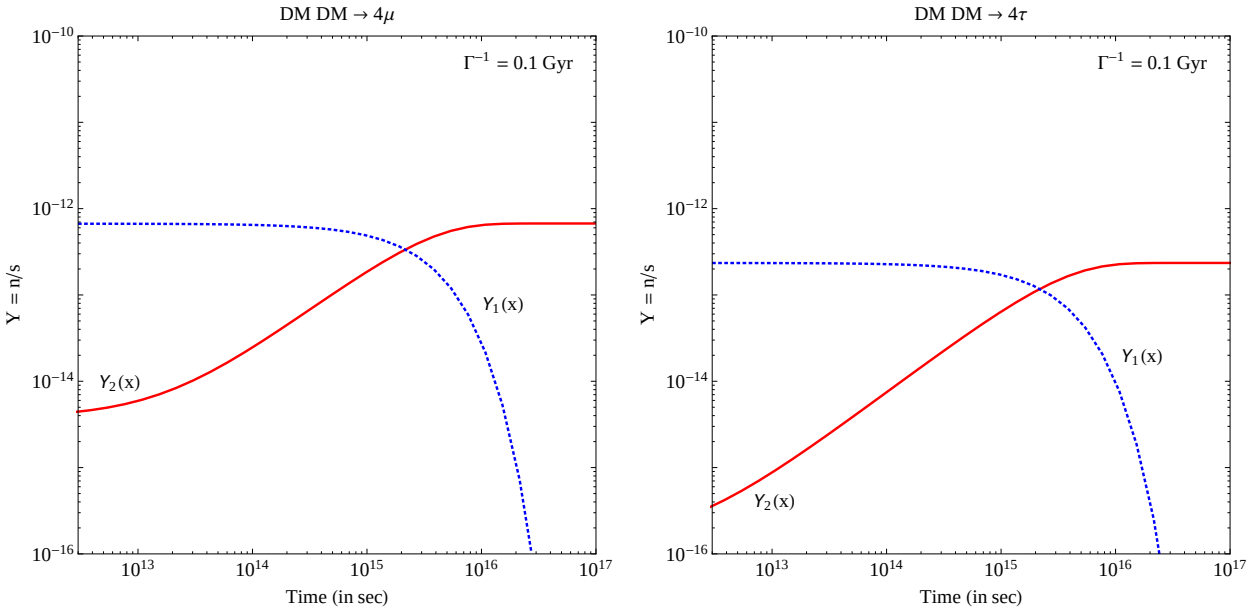

FIG. 3: The yield $Y \equiv n/s$ of χ_1 and χ_2 as a function of time, assuming a lifetime of χ_1, $\Gamma^{-1} = 0.1$ Gyr. The annihilation cross-sections are taken to be $\langle\sigma_1 v_1\rangle = 2.2 \times 10^{-26}$ cm^3 s^{-1} and $\langle\sigma_2 v_2\rangle = 4.57 \times 10^{-24}$ cm^3 s^{-1} for annihilation of χ_2 to 4μ (left plot) and $\langle\sigma_2 v_2\rangle = 3.63 \times 10^{-23}$ cm^3 s^{-1} for annihilation to 4τ (right plot). The late time decay of χ_1 populates χ_2 with the correct dark matter relic abundance. At early times, the abundance of χ_2 is suppressed by a factor of $\mathcal{O}(10^{-2} - 10^{-3})$ compared to its present day abundance.

B. Constraints on the LD2DM scenario from cosmology

There are two types of cosmological constraints that arise on the LD2DM scenario: energy deposition constraints (arising from CMB observations) and structure formation constraints. The first constraint imposes a lower bound on the decay lifetime of χ_1 and the latter constrains the mass splitting between the two DM species. We will discuss each of these constraints in turn.

1. Late time energy deposition constraints

The late time population of the lighter dark matter particle χ_2 (created by the decays of χ_1) will also undergo annihilations. These annihilations lead to energy deposition into the thermal plasma in the early universe. For lifetimes of χ_1 much smaller than than the age of the universe at recombination ($380,000$ years or 10^{13} s), the light species χ_2 behaves similarly to a conventional WIMP. Its annihilations in the early universe would lead to energy deposition into the thermal plasma, changing the ionization history of the universe and broadening the surface of last scattering. As discussed in Sec. II B, this would predict a distortion of the CMB temperature and polarization anisotropy spectra, which upon comparison with observations, would rule out the large annihilation cross-sections of χ_2 needed to explain the positron excess.

However for lifetimes of χ_1 greater than the age of the universe at recombination ($\Gamma^{-1} \gtrsim 10^{13}$ s) we expect that the epoch of annihilations of χ_2 will be postponed, leading to late time energy depositions which will alter the ionization history of the universe during the cosmic "dark ages". This altered ionization history can also be probed by its influence on the anisotropy spectrum of CMB radiation as it travels from the surface of last scattering towards us. Rather than constraining the annihilation cross-section at a particular epoch (like the recombination era constraints discussed in Sec. II B) or by looking at the effect on single observables like the total optical depth (arising from very late decays), Ref. [86] employs a principal component analysis to provide a bound on the DM annihilation cross-section by considering the complete shape of the ionization history determined by an input cosmological model. Since our scenario has a novel energy deposition history compared to the standard s-wave annihilating dark matter, the principal component approach is a useful method to provide a robust bound on the annihilation cross-section of DM from CMB observations.

We start by discussing the case of a standard thermal relic produced via freeze-out (the conventional WIMP scenario). Post freeze-out, residual dark matter annihilations inject energy into the thermal plasma (or the intergalactic medium (IGM) at late times). These annihilations have an energy injection rate per comoving volume given by,

$$\left.\frac{dE}{dtdV}(z)\right|_{\text{injected}} = \kappa \left(2m_{\text{DM}}c^2\right) n^2(z)\langle\sigma v\rangle, \tag{7}$$

where $\kappa = 1/2$ for majorana-like DM and $\kappa = 1/4$ for Dirac-like DM. Here, z is the redshift at which the annihilation occurs, m_{DM} is the mass of the dark matter particle, $n(z)$ is the number density of DM particles and $\langle\sigma v\rangle$ is the velocity-averaged annihilation cross-section.

For a standard thermal relic, its cosmological abundance at a redshift z is given by,

$$n_{\text{TR}}(z) = \frac{\rho_c}{m_{\text{DM}}}\Omega_{\text{DM}}(1+z)^3, \tag{8}$$

where ρ_c is the critical density and $\Omega_{\text{DM}} \sim 0.2$ is the present day dark matter energy density fraction.

This *energy injection* via dark matter annihilations does not however give the correct *energy deposition* history. To get the correct energy deposition history one needs to include a redshift dependent efficiency factor $f(z)$, defined such that,

$$\left(\frac{dE}{dtdV}\right)_{\text{deposited}} = f(z)\left(\frac{dE}{dtdV}\right)_{\text{injected}}. \tag{9}$$

The detailed derivation of the factor $f(z)$ has been shown in [86]. We highlight here some key factors that determine $f(z)$ and write down the final expression without repeating the derivation.

1. In Ref. [86] it was shown that energy E injected in photons and positrons at an early redshift z_{inj} will only be deposited as ionizing radiation at a later redshift z_{dep}. The

author provided tables of the fractional energy deposited as a function of initial energy for various injection and deposition redshifts, $T(z_{\rm dep}, z_{\rm inj}, E)d\ln(z_{\rm dep})$[6], for various electromagnetic species (photons and electron-positron pairs).

2. The energy injection formula we are considering only includes annihilations from the smooth, isotropic component of dark matter. One needs to include a boost factor $\mathcal{B}(z)$ due to halo formation at late times, which enhances the dark matter annihilation probability as compared to the smooth component alone.

3. An effect that is new in the LD2DM scenario as compared to previous studies of energy deposition constraints, is that the number density of annihilating dark matter particles in our scenario differs from the standard thermal relic scenario[7]. Recall that the "active species", χ_2 is produced initially with a very low abundance due to freeze-out and is later repopulated via the decay of χ_1.

Thus in the LD2DM scenario, a clearer definition of $f(z)$ is provided by,

$$\left(\frac{dE}{dtdV}\right)_{\rm deposited,smooth+halos,LD2DM} = f(z)\left(\frac{dE}{dtdV}\right)_{\rm injected,smooth,TR}. \tag{10}$$

Note that as a normalization convention, we choose the injected energy to originate from a smooth thermal relic, however when calculating the deposited ionizing energy (which affects CMB observables) we are considering all of the factors listed above.

The resulting formula for $f(z)$, after taking these effects into account, is given below,

$$f(z) = \frac{H(z)}{(1+z)^3} \times \frac{\sum\limits_{\rm species(s)} \int \frac{(1+z')^2 dz'}{H(z')}\left(1+\mathcal{B}(z')\right)\left(\frac{n_2^2(z')}{n_{\rm TR}^2(z')}\right)\int T_s(z', z, E_s) E_s \frac{d\bar{N}_s}{dE_s} dE_s}{\sum\limits_{\rm species(s)} \int E_s \frac{d\bar{N}_s}{dE_s} dE_s}. \tag{11}$$

Here, $H(z)$ is the Hubble parameter and $\frac{d\bar{N}_s}{dE_s}$ is the spectrum of particles of type s (e^+e^- pairs or photons) per annihilation. The boost factor due to halos is given by [88],

$$\mathcal{B}(z) = \frac{\bar{f}_h}{(1+z)^3}{\rm erfc}\left(\frac{1+z}{1+z_h}\right), \tag{12}$$

where z_h is the redshift at which halos start to contribute an enhancement to the DM annihilations and f_h is proportional to a halo "concentration function". Following Ref. [88], we take $\bar{f}_h = 10^9$ and $z_h = 20$. We take the comoving number density of χ_2 (n_2) as computed

[6] These energy deposition fractions were updated in Ref. [87] to correctly account for different energy deposition channels (ionization, heating and excitation of the gas and low energy photons which would distort the CMB spectrum). Our interest here is only the ionization channels of Ref. [87], which we use to compute the corrected ionizing energy deposition fractions.

[7] In Ref. [86], a somewhat similar situation was considered in the case of oscillating asymmetric dark matter.

in Sec. IV A and $n_{\rm TR}$ is the comoving number density of a thermal relic. Note that the factor $\left(\frac{n_2^2(z')}{n_{\rm TR}^2(z')}\right)$ is unique to the LD2DM scenario, and it arises because of the alternate cosmological history of χ_2. We were able to numerically compute the energy deposition efficiency factor $f(z)$ using the Mathematica [89] tools provided by [86]. For each final state, the energy injection spectrum $\frac{d\bar{N}_s}{dE_s}$ into photons, electrons and positrons is different. We used the PPPC4DMID to obtain the spectrum for the e^+e^- pairs and photons in different annihilation channels (4μ, 4τ). We then computed $f(z)$ for each annihilation channel for different values of the heavy species decay lifetime Γ^{-1} (which controls the abundance $n_2(z)$ of χ_2).

Once we obtained the efficiency factor $f(z)$, we were able to compute the ionizing energy deposition history for various annihilation cross-sections $\langle\sigma_2 v_2\rangle$. Next, we examined CMB constraints on this energy deposition history. Ref. [86] used a principal component analysis (PCA), first developed in [90], to constrain the energy deposition history and consequently the annihilation cross-section. We followed the same approach to constrain the annihilation cross-section $\langle\sigma_2 v_2\rangle$. Using a modified version of the Mathematica code provided by [86], we computed the upper bound on the annihilation cross-section $\langle\sigma_2 v_2\rangle$ for different values of the lifetime of χ_1.

We note here a subtlety of our analysis: for compatibility with the PCA approach we assumed that the cross-section $\langle\sigma_2 v_2\rangle$ only enters the energy deposition history *linearly*. However, this is not really the case in the LD2DM scenario since the abundance $n_2(z)$ at early times is also controlled by $\langle\sigma_2 v_2\rangle$. We will ignore this subtlety by using a fixed cross-section in the calculation of $n_2(z)$ (We choose the best fit cross-sections needed to explain the AMS-02 positron excess). Another issue is that the PCA approach that we consider does not provide the most reliable bound on energy deposition when the lifetime of χ_1 is of the order of the age of the universe today ($\Gamma^{-1} \geq 10^{16}$ s). This is because for such late time energy depositions astrophysical processes contribute to ionization of the IGM and this contribution must be accounted for when setting a constraint on the DM annihilation cross-section. For such late time decays, we expect the bounds on the annihilation cross-sections from other sources, such as the heating of the IGM to also be important [91, 92].

Our resulting upper bounds on $\langle\sigma_2 v_2\rangle$ as a function of the lifetime Γ^{-1} are shown in in Fig. 4 (left panel) for the 4μ annihilation channel and in Fig. 4 (right panel) for the 4τ annihilation channel. We also plot the required annihilation cross-section necessary to explain the AMS-02 positron excess for comparison. For short lifetimes of χ_1 (smaller than the time of recombination, $\Gamma^{-1} < 10^{13}$ s), we see that the bound saturates to a constant value as expected in the case of a standard WIMP type scenario. In this case, the bound primarily arises due to the effect on CMB anisotropies from the broadening of the surface of last scattering. As we have already seen in Sec. II B, the resulting constraint rules out the annihilation cross-sections needed to explain the positron excess in either the 4μ or the 4τ channel. However for both annihilation channels, for lifetimes greater than $\sim 10^{13}$ s, we find that the late time energy deposition constraints are less stringent and the required annihilation cross-sections to explain the AMS-02 positron excess are consistent with the resulting CMB bounds.

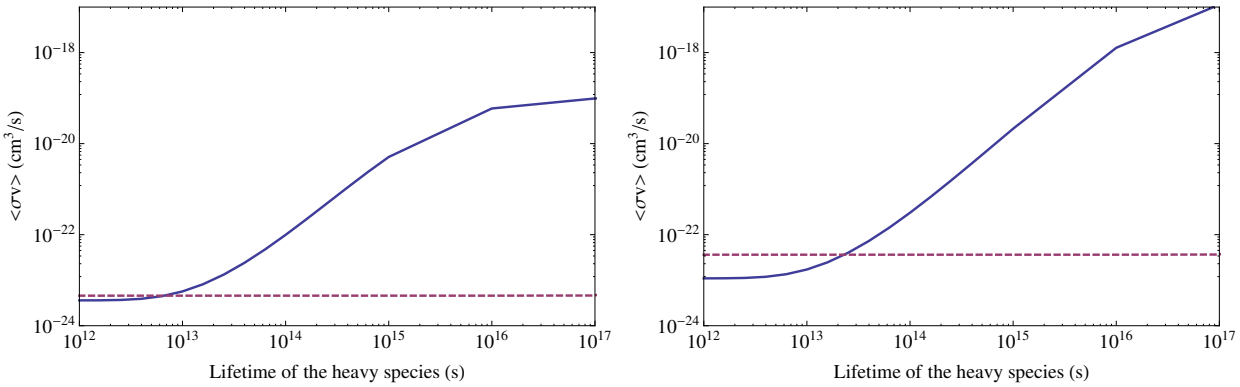

FIG. 4: Upper bound on the annihilation cross-section (solid blue curve) of χ_2 to 4μ (left plot) and 4τ (right plot) from the energy deposition history constraints arising from observations of the CMB. Also shown is the required annihilation cross-section to explain the AMS-02 positron excess for each case (dashed magenta line).

2. *Structure formation constraints*

In the LD2DM scenario the daughter particles (χ_2) receive a kick velocity v_k in the frame of the mother particles (χ_1) which is proportional to the mass difference $\Delta m \equiv m_1 - m_2$ between χ_1 and χ_2,

$$v_k = \frac{\Delta m}{m_1} c, \tag{13}$$

where c is the speed of light. The resultant kick velocity strongly impacts the structure formation process in the universe. The free streaming length of the dark matter suddenly increases after the decay of χ_1, suppressing all structure below the enhanced free streaming length scale. Using Lyman-α forest data, Ref. [93] finds that the kick velocity, v_k, received by the daughter particles is restricted to be less than 40 km/s for $\Gamma^{-1} < 10$ Gyr. Thus the the strong constraints on v_k essentially restricts the mass of χ_1 to be nearly degenerate with χ_2 with $\Delta m \lesssim 0.1$ GeV.

V. A TOY MODEL FOR THE BASIC LD2DM SCENARIO

In the basic LD2DM scenario laid out in Sec. IV, χ_1 forms the primordial dark matter which decays to χ_2 over cosmological timescales. As we have seen in Sec. IV B, generic constraints from small scale structure and late time energy deposition force us to consider the mass of χ_1 to be nearly degenerate with χ_2, $\Delta m = m_1 - m_2 \lesssim 0.1$ GeV and the lifetime of χ_1, $\Gamma^{-1} \gtrsim 10^{13}$ s. In this section, we will describe a toy model which realizes the basic LD2DM scenario.

We will assume that χ_1 and χ_2 are both Dirac fermions. We introduce two more fields in our toy model, (1) a dark radiation component (ϕ), which is a light complex scalar field that will play the role of the thermal bath for the annihilation of χ_1, and (2) a massive dark force carrier Z' that mediates the annihilation of χ_2 to four leptons.

The interaction terms in the Lagrangian for the effective theory are given by,

$$\mathcal{L}_{\rm int} = -\frac{1}{\Lambda}\overline{\chi}_1\chi_1\phi\phi^* - ig_\phi(\phi^*\partial^\mu\phi - \phi\partial^\mu\phi^*)Z'_\mu - ig\overline{\chi}_2\gamma^\mu\chi_2 Z'_\mu - ig'\overline{\psi}_\ell\gamma^\mu\psi_\ell Z'_\mu + y\overline{\chi}_1\chi_2\phi + \text{ h.c.} \tag{14}$$

Here ℓ denotes the heavy SM leptons (either μ or τ). The couplings of the Z' to χ_2, ℓ and ϕ are denoted by g, g' and g_ϕ respectively. We will assume a hierarchy $g \gg g' \gg g_\phi$. This hierarchy of couplings ensures that the annihilation to on-shell Z's which decay to SM leptons is the dominant annihilation channel for χ_2 ($\chi_2\chi_2 \to Z'Z' \to 4\ell$ as opposed to $\chi_2\chi_2 \to Z' \to 2\ell$ or $\chi_2\chi_2 \to Z'Z' \to 4\phi$).

For χ_1 the dominant annihilation channel is to dark radiation ϕ, ϕ^*. The interaction term is written as an effective theory operator with Λ denoting the ultraviolet scale of this effective theory. The dark radiation provides a thermal bath for the the freeze-out of χ_1 and is kept in equilibrium with the SM thermal bath in the early universe through the interaction with μ (or τ) (via the Z').

The last term in the interaction Lagrangian violates the $\mathbb{Z}_2$ symmetry of χ_1 and χ_2 and allows χ_1 to decay into χ_2 and ϕ. In order for the lifetime of χ_1 to be of the order of cosmological timescales, the coupling y must be extremely small. We can estimate the decay width of the heavy dark matter particle χ_1 as,

$$\Gamma \sim \frac{y^2}{4\pi}(m_1 - m_2). \tag{15}$$

Thus, in order for the lifetime to be of the order of 0.1 Gyr ($\sim 10^{16}$ s), for a mass-splitting of $\mathcal{O}(0.1)$ GeV, we find that $y \sim 10^{-11}$.

Our toy model makes some minimal assumptions for economy of particle content:

- One key assumption is that the particle that makes up the dark sector thermal bath that χ_1 annihilates to while undergoing freeze-out is the same as the particle ϕ involved in the decay $\chi_1 \to \chi_2 + \phi$.
- The second minimal assumption is that the mediator Z' that is responsible for the annihilation of χ_2 to 4 leptons is also responsible for keeping the dark radiation bath in kinetic equilibrium with the visible sector (at least in the early universe).

These assumptions can be relaxed without affecting our basic scenario. In fact, it is not necessary that χ_1 is produced via freeze-out as long as it has the correct relic density before it starts decaying to χ_2.

As emphasized in Sec. IV the basic LD2DM scenario has five key parameters. The masses and annihilation cross-sections of χ_1 and χ_2 and the lifetime of χ_1. Specializing to the toy model, we see that the mass of χ_2 must be taken to be $m_2 = 570$ GeV ($m_2 = 1700$ GeV) for annihilation to 4μ (4τ), as required to explain the shape of the positron spectrum observed by the AMS-02 experiment (See Tab. 1). The coupling g controls the annihilation cross-section $\langle\sigma_2 v_2\rangle$ and is fixed by the normalization of the excess positron flux, $1/\Lambda$ controls the annihilation cross-section $\langle\sigma_1 v_1\rangle$ and is fixed by the thermal freeze-out value[8] and y controls the lifetime of the decay $\chi_1 \to \chi_2 + \phi$ which is constrained by CMB observations.

[8] We point out that the value of Λ needed to achieve the thermal relic cross-section would be close to the

The rest of the parameters and fields introduced in the toy model could potentially gives rise to (or be constrained by) cosmological observations and signatures at terrestrial experiments. We will briefly address these below:

- If the Z' couples to muons, this coupling would be strongly constrained by muon $g-2$ measurements and must therefore be small.

- The dark radiation contributes to the number of effective neutrinos $\Delta N_{\rm eff}$ measured by CMB experiments, however the exact contribution depends on the temperature of the radiation bath relative to the visible sector bath at the epoch of recombination. This temperature is controlled by the efficiency of the $\phi - \mu$ (or $\phi - \tau$) scattering process which also depends on the Z' coupling to muons. If this coupling is small, the dark radiation bath decouples early and has a low temperature as compared to CMB photons which are heated by annihilating particles such as e^+e^- pairs. This would result in a negligible contribution to $\Delta N_{\rm eff}$.

- We could also consider ϕ to be a visible sector particle in which case the only candidates are photons and neutrinos, due to the small mass splitting between χ_1 and χ_2 (we would have to change the spins of χ_1 and χ_2 in our toy model in either of these cases). Photons would again be subject to energy deposition constraints from decaying dark matter and are hence disfavored [86]. However, the case where ϕ is a neutrino is interesting and could lead to features in the Cosmic Neutrino Background at energies of $\mathcal{O}(\Delta m/(1+z_d))$, where z_d is the characteristic redshift for the decay of χ_1.

Apart from these experimental and observational issues, we run into two main fine-tuning problems when trying to build a detailed particle physics model that realizes the basic LD2DM scenario, as can be seen in the parameters of our toy model.

- The decay lifetime of χ_1 is of the order of the age of the universe, which implies that the coupling responsible for this decay is very small and hence highly tuned.

- The mass splitting between χ_1 and χ_2 is extremely small, with $\epsilon \equiv \frac{\Delta m}{m_1} \sim 10^{-4}$.

The first fine tuning problem could potentially be solved by positing a $\mathbb{Z}_2$ symmetry for χ_1 that is broken spontaneously but communicated through loops or via highly suppressed mass scales. The second fine tuning is more problematic because χ_1 and χ_2 have different effective couplings to SM muons or taus and hence they receive different quantum corrections to their masses.

We emphasize here that in this work we have merely highlighted some interesting implications of models that incorporate the basic LD2DM scenario. We leave a detailed development of the toy model and various extensions, along with a full analysis of their parameter space and particle phenomenology to future work.

---

mass scale m_1 implying a breakdown of the effective theory description of this annihilation process. We take this to imply the existence of a new light mediator for this interaction, but we will avoid introducing the mediator explicitly.

VI. POSSIBLE COSMOLOGICAL FEATURES OF THE TOY MODEL

In this section we will discuss several small scale structure and cosmological problems and show that the toy model discussed in the previous section has the potential to resolve these problems.

A. Impact on small scale structure

The cold dark matter (CDM) paradigm has been very successful in explaining the large scale structure of the universe but on small scales there are hints from observations of dwarf galaxies of the Milky Way (MW) and M31 that something may be lacking in this description. Precision observations of dwarf galaxies show DM distributions with cores, in contrast to cusps predicted by CDM simulations ("cusp-core" problem) [94]. It has also been shown that the most massive subhalos in CDM simulations of MW size halos have higher central densities than those observed in the brightest satellites of the MW ("too big to fail problem") [52]. Simulations also predict numerous dwarf satellites that are not seen ("Missing Satellite Problem") [47, 48]. The "missing satellite problem" could potentially be explained by our failure to detect ultra faint dwarf satellites [95] in the MW. However, several potential solutions to these small scale structure problems that rely on the inclusion of baryonic physics in DM halo dynamics have also been proposed. For example, the "missing satellite problem" could alternatively be explained by baryonic processes which inhibit the accretion of gas in low mass subhalos [96, 97]. Similarly, [98] found that baryonic processes like episodic supernova feedback can potentially flatten the cuspy DM profile at the center of a halo, but it is unlikely that the "too big to fail" problem can be resolved by such processes alone [99]. It is also worthwhile to consider the predictions of alternative dark matter physics for these issues (see [100] for review).

Models which subscribe to the LD2DM paradigm (including the toy model we proposed in the last section) consist of two approximately degenerate DM particles χ_1 and χ_2. The heavy species χ_1 would undergo decay on a time scale (possibly) of the order of the age of the universe producing χ_2 with a non-relativistic kick velocity v_k. As a result, dark matter halos which have a maximum circular velocity, V_{max}, close to the value of the kick velocity are disrupted once significant decay has occurred. From the Lyman-α constraints discussed in Sec. IV B, we find that the allowed values of v_k for Γ^{-1} less than the age of the universe are of the order of 10 km/s. This is around the order of the typical V_{max} values found in dwarf galaxies. Hence, the effect of a kick velocity imparted during decay of the heavy DM species would be most readily visible through its impact on our galactic halo substructures. Subhalos which have V_{max} less than v_k will almost completely disintegrate after all the mother particles have decayed. Simulations of a MW sized halo using models where an unstable dark matter particle decays into a stable non-interacting dark matter particle were performed by [101], and they found a significant reduction of subhalo count for $\Gamma^{-1} = 1$ Gyr and 10 Gyr and $v_k = 20$ km/s. This indicates that decaying dark matter has the potential to solve the "Missing Satellite Problem" for an appropriate choice of v_k (or a corresponding choice of the mass splitting). For $V_{max} >> v_k$ almost no impact should be felt by the subhalos. However, subhalos which have V_{max} slightly greater than v_k will experience expansion due to the sudden injection of energy into the system through decays. The subhalos will also suffer from some fraction of mass loss as some initially loosely bound

particles will decay to particles that are no longer bound to the subhalo. The net effect is that there will be a reduced central halo density [44]. However, this effect is only dominant for values of V_{max} close to v_k. Ref. [101] found that $\Gamma^{-1} = 10$ Gyr and $v_k = 20$ km/s sufficiently drove down the central density of the largest subhalos in the simulations, which they concluded would resolve the "too big to fail" problem, although the density profiles still remained cuspy.

B. Impact on Hubble tension and σ_8 tension

Recently, it has been observed that the Planck best fit parameters assuming the concordant ΛCDM cosmological model [19] prefer σ_8 and H_0 values which are different from the values that are inferred from direct observations. In particular, Planck prefers a value of H_0 which is smaller than the Hubble Space Telescope (HST) measurement [102], while the preferred σ_8 value is larger than the directly measured value extracted from observations of large scale structure [103]. While it is premature to rule out the contribution of underestimated systematic errors on the direct measurements in these discrepancies, they still motivate theories beyond the standard ΛCDM scenario. The toy model we considered in Sec. V allows room for additional interactions between a dark radiation component (ϕ) and a primordial dark matter particle (χ_1), which under certain conditions could potentially resolve the tensions in the H_0 and σ_8 measurements simultaneously. We will elaborate on this resolution below.

In the early universe, when all the neutrinos are relativistic, the effective number of neutrinos, $N_{\rm eff}$, can be defined as a proxy variable to describe the total radiation energy density (ρ_r) in terms of the photon energy density ρ_γ:

$$\rho_r = \rho_\gamma + \rho_\nu + \rho_{\rm DR} \equiv \left[1 + \frac{7}{8}\left(\frac{4}{11}\right)^{4/3} N_{\rm eff}\right]\rho_\gamma, \tag{16}$$

where, ρ_ν and $\rho_{\rm DR}$ are the densities of neutrinos and a putative dark radiation component respectively. In the standard ΛCDM scenario where the dark radiation component is absent, $N_{\rm eff}$ has a nominal value of 3.046 [104]. The addition of dark radiation in our toy model would increase $N_{\rm eff}$ as,

$$\Delta N_{\rm eff} = N_{\rm DR}\left(\frac{T_{\rm DR}}{T_\nu}\right)^4 \times \begin{cases} 8/7 \text{ (bosonic DR)} \\ \\ 1 \text{ (fermionic DR)} \end{cases}. \tag{17}$$

Here, $T_{\rm DR}$ and T_ν denote the temperatures (at recombination) of dark radiation and neutrinos respectively. Thus, an increase in dark radiation would lead to an increase in the parameter $N_{\rm eff}$. Such an increase in $N_{\rm eff}$ due to dark radiation can be compatible with the observed CMB data provided that the characteristic redshifts of matter/radiation equality and matter/cosmological constant equality remain unchanged. This can be accommodated by an appropriately larger value of H_0. A recent analysis found that an extra dark radiation component with $\Delta N_{\rm eff} \approx 0.4 - 1$ can in fact reconcile the measurements from HST with Planck data [105]. This is also compatible with big bang nucleosynthesis constraints on extra relativistic degree of freedom, $\Delta N_{\rm eff} \leq 1$ at 95% C.L (see [106]). Thus, it is clear that

the data is consistent with the inclusion of an extra dark radiation component (as in our toy model) in the universe and this would also allow for a resolution to the H_0 tension.

Although an increase in $N_{\rm eff}$ alleviates the tension in H_0, it would also exacerbate the σ_8 tension by increasing the best fit value obtained from CMB data [19]. Such a conflict could be resolved by introducing a drag force between dark radiation and dark matter for which the interaction rate scales with the Hubble parameter during the radiation dominated era [107]. This coupling essentially restricts the growth of dark matter over-densities at all scales within the Hubble horizon during the radiation dominated era. This also ensures that the scales crossing the Hubble horizon during the matter dominated era will remain unaffected as the Hubble rate is larger than the interaction rate in this epoch. Hence, the power spectrum on relatively small scales (including $8/h$ Mpc) could potentially be suppressed, which would reconcile the inferred value of σ_8 extracted from the normalization of the CMB power spectrum with the directly obtained value from observations of large scale structure. Thus, introducing a drag force of this type between the primordial dark matter χ_1 and dark radiation in our toy model could potentially resolve the σ_8 tension as well.

VII. SUMMARY AND DISCUSSION

The high-precision data for the cosmic positron flux released recently by AMS-02 provides a unique opportunity to investigate a dark matter interpretation of the observed positron excess without modeling the primary electron spectrum. In this work, we revisited the best fit cross-section and mass needed for a leptophilic DM candidate to explain the observed positron excess. We implemented the latest propagation profiles and an updated model for the galactic magnetic field model in the Dragon code to solve the propagation equation numerically, obtaining an improved fit for our calculated positron flux in the leptophilic DM annihilation channels that we considered.

We compared these best-fit parameters with constraints arising from the observed gamma ray flux from dwarf galaxies and diffuse gamma ray measurements. We found that DM annihilation to either the 4μ or 4τ channels was still allowed by these constraints. However, the most stringent constraints on such a dark matter candidate would arise from observations of the CMB. As we have argued, if an s-wave annihilating dark matter species exists before the epoch of recombination, it would deposit energy into the thermal plasma in the early universe with observable effects on the CMB temperature and polarization power spectra. The large cross-section needed to explain the positron excess would certainly be ruled out, putting an annihilating DM interpretation of the positron excess in serious jeopardy.

The main feature of this work was our proposal of a novel paradigm, which we dubbed the late-decaying 2-component dark matter (LD2DM) scenario. In this scenario, there is a heavy dark matter species, χ_1, that annihilates with a low (thermal relic) cross-section, while decaying on cosmological time scales to a more strongly annihilating lighter DM species, χ_2. We posit that χ_2 plays the role of DM in the present universe and its annihilations give rise to the observed positron excess. We showed through an explicit calculation of the yields that the LD2DM scenario can give rise to the correct relic abundance of DM in the present universe while evading CMB constraints on energy deposition during the epoch of recombination.

We then proceeded to examine constraints that arise on the LD2DM scenario from cosmol-

ogy, specifically (1) constraints arising from *late-time energy depositions* during the cosmic dark ages and their effect on the CMB and (2) structure formation constraints on decaying dark matter. We found that these constraints force us to consider χ_1 to be a long lived DM candidate with a a lifetime greater than $\sim 10^{13}$ s and a very small mass splitting between χ_1 and χ_2.

For concreteness, we presented a toy particle physics model that realizes the basic LD2DM scenario and briefly discussed possible observations, constraints and fine-tuning issues in this model. We also explored several possible cosmological implications of this toy model, such as the possibility to solve certain small scale structure problems and the potential to resolve the tension between the values of σ_8 and H_0 extracted from CMB observations with those from low-redshift measurements.

In this work we have left open several avenues that could be pursued if the basic LD2DM paradigm is taken seriously as an explanation of the positron excess. We highlight below some directions for future work:

DM and the positron excess: The very first question that needs to addressed is whether the observed positron excess will continue to favor a dark matter interpretation once more data is collected. The AMS-02 detector is designed to continue collecting data through 2020, so future releases of data will improve precision in the high energy bins and reveal the shape of the positron fraction (flux) that may help in distinguishing between astrophysical and DM interpretations of the excess [73]. Also, as advocated by [108], determining the energy-dependent anisotropy of the incoming positrons may be an indicator of the nature of its source: a high anisotropy would favor a single-source hypothesis while a DM interpretation is better served by an isotropic positron source.

Particle physics models of the LD2DM scenario: We leave a detailed development of the toy model and various extensions, along with a full analysis of the parameter space and particle phenomenology to future work. One potentially promising phenomenological avenue is to look at scenarios where χ_1 decays to χ_2 and a neutrino. This could lead to observable signatures in the Cosmic Neutrino Background. On the model building side, it would be interesting to see whether the fine tunings in our toy model can be explained by embedding it in a UV completion.

21cm astronomy and Epoch of Reionization: It is interesting to consider the LD2DM scenario for a decay lifetime of χ_1 of the order of the age of the universe. χ_2 has a significantly larger cross-section compared to the vanilla WIMP particle and hence can have a substantial contribution in saturating the optical depth to reionization. On top of that, χ_2 also has a varied abundance history which will cause its energy deposition record to be different from that of conventional ΛCDM cosmologies. Hence, we expect the LD2DM scenario to leave a distinct imprint on the reionization history of the universe. The observations of redshifted 21cm radiation from the Epoch of Reionization (EoR) will be essential in providing constraints on the contribution to reionization process from various sources including DM annihilation. The ongoing experiments like HERA [109] are expected to provide us with exciting information like global history of EoR progression, but they will only be limited upto $z \approx 11$. In the future, experiments like SKA [110] will have much better sensitivity, redshift coverage (upto $z \approx 30$) and resolution which will help shed light on the dark ages. It will also play a major role in probing the alternate reionization histories as maybe the case in the LD2DM scenario.

Acknowledgments

We are grateful to Andre Scaffidi for providing the constraint plot for 4μ channel after including radiative corrections using the newest Fermi-LAT likelihoods from `Pass 8` data. We thank Marco Cirelli, Basudeb Dasgupta, Fabio Iocco, and Rishi Khatri for useful discussions. We especially thank Tracy Slatyer for helpful correspondence on the PCA constraints for late time dark matter annihilations. JB would like to acknowledge the hospitality of Mainz Institute for Theoretical Physics (MITP) where a part of this work was completed. The work of VR was supported by an IRCC, IIT-B seed grant.

Appendix A: Cosmic Ray Propagation in the Galaxy

1. Propagation equation and parameters

Irrespective of the source of their production, charged cosmic rays (CRs), positrons in our case, propagate through the turbulent magnetic field in our galaxy where they get deflected by random inhomogeneities. As they propagate they also lose energy through several processes such as synchrotron radiation, bremsstrahlung, possible reacceleration or convection and from undergoing inverse Compton scattering (ICS) on the CMB and ambient starlight. Ignoring the losses through fragmentation and radioactive decay, CR transport can be modelled by a diffusion equation for each CR species [58],

$$\frac{\partial \psi}{\partial t} = Q(x,p) + \nabla.(D_{xx}\nabla\psi - V_c\,\psi) + \frac{\partial}{\partial p}p^2 D_{pp}\frac{\partial}{\partial p}\frac{1}{p^2}\psi - \frac{\partial}{\partial p}\left[\dot{p}\psi - \frac{p}{3}(\nabla.V_c)\psi\right], \qquad \text{(A1)}$$

where $\psi(x,p,t)$ is the spatial density of CRs per unit momentum interval (p) , $Q(x,p)$ is the source distribution, D_{xx} and D_{pp} are the diffusion coefficients in position and momentum space respectively, $V_c(z)$ is the convection velocity (assumed to vary only along the height of the galactic disk) and $\dot{p}$ denotes an energy loss coefficient. The spatial diffusion coefficient is conventionally taken to be position-independent and is parameterized by a power law $D_{xx} = D_0\,(R/R_0)^{\delta}$, where $R \equiv pc/Ze$ is the rigidity of the particle and δ is the power law dependence of D on energy. The coefficient of diffusive reacceleration in momentum space, D_{pp}, is a function of the velocity of hydrodynamical disturbances also called the Alfvèn wave speed, v_A, and the relation is given by,

$$D_{pp} = \frac{4p^2 v_A^2}{3\,D_{xx}\delta(4-\delta^2)(4-\delta)}. \qquad \text{(A2)}$$

The energy loss coefficient, $\dot{p}$, takes into account all energy losses mentioned above (for details of the various contributions see Ref. [111]). In particular we note that the synchrotron losses depend on the modelling of the Galactic Magnetic Field (GMF), as outlined in Appendix A 3.

Eq. (A1) can be solved numerically using codes such as Galprop [112] and Dragon [57], or semi-analytically which gives a better handle on the input parameters. Both these techniques proceed by modelling the diffusive region of the galaxy as a two-dimensional cylinder extending radially upto 20 kpc, with height $2L$ in the vertical direction. The boundary condition is imposed such that the quantity ψ vanishes at $z = \pm L$ implying that CRs can escape freely beyond the boundaries of the cylinder. The height of the cylinder L can vary

between 1 - 15 kpc for different propagation models, however, recent combined analyses of synchrotron emission and γ-ray data strongly disfavour models with $L < 2$ kpc [113, 114].

Notice that we still need to fix the major propagation parameters $(D_0, \delta, L, dV_c/dz, v_A)$. This is done by fitting-to-data the secondary-to-primary Boron-to-Carbon (B/C) ratio and the unstable-to-stable Beryllium ratio (^{10}Be/^{9}Be) in cosmic rays as they are largely independent of the injection spectra, and then extracting the best fit values of the parameters for each propagation model. While computing the value of these parameters by doing a global Bayesian fit using statistical techniques such as the Markov Chain Monte-Carlo (MCMC) scan [115, 116] minimizes the systematic error in an analysis, popular models available in the market, the MIN-MED-MAX profiles [67, 68] for instance, are generally adopted for convenience or for consistency with previous results [111]. In our analysis, we adopt two benchmark models for propagation from [58] and [69]. The parameters appearing in the diffusion equation for the models we consider are presented in Tab. 2. The models themselves are briefly described below.

- Model A (MODA) is a propagation model that also includes *diffusive convection* along with other energy-loss mechanisms. So, there is an additional parameter for the galactic convective wind, V_c, that is switched on in the global fit. As data, the authors of [58] use measurements of the B/C ratio from AMS-02 and ACE, and the ^{10}Be/^{9}Be ratio from experiments ACE, Balloon, IMP7&8, ISEE3HKH, ISOMAX, Ulysses-HET and Voyager to constrain the propagation parameters. Also, to fit the low-energy B/C data they adopt a momentum-independent diffusion coefficient below $R_0 = 4.71$ GV by setting $\delta = 0$.

- Model B (MODB) includes *diffusive reacceleration* instead of convection. Motivated by [115, 116], the authors of [69] use reacceleration (implemented in Dragon through the "Ptsukin03" parametrization derived from [117]) as a mechanism to reproduce the observed peak in the B/C spectrum. Subsequently, they perform a global Bayesian fit using a MCMC scan over the latest AMS-02 B/C and proton data to constrain their propagation model, and find that the uncertainties in the parameters are greatly reduced as compared to previous analyses. An interesting conclusion they make is that a relatively thin diffusive halo size is favored by the AMS-02 data.

TABLE 2: Propagation parameters for profiles MODA, MODB based on [58] and [69] respectively.

Parameters	Model A	Model B
D_0 (10^{28}cm^2/s)	1.95	6.464
δ	0/0.51	0.29
R_0 (GV)	4.71	4
L (kpc)	2.5	3.2
dV_c/dz (km/s)	4.2	-
v_A (km/s)	-	44.7

2. Parameters for Input Injection Spectra

The total positron flux can be expressed as the sum of a secondary astrophysical background and a primary component from DM annihilations. The secondary component is produced by the spallations of CR nuclei on the ISM. In order to compute the secondary positron component, we first need to set the nuclear CR source parameters in Dragon as described below. The steady state CR flux after propagation is then used to numerically compute the secondary positron source term (Q_{e^+}) by following the parametrization for secondary pion production in spallations developed by [118].

The source term for every CR nuclear species is given by

$$Q_i(E_k, r, z) = f_S(r, z)\, N_i \left(\frac{R}{R_{\rm br}}\right)^{-\gamma_i}, \tag{A3}$$

where i denotes the nuclear species, R is the rigidity of the particle, γ is a power law index that may have different values above and below $R_{\rm br}$, and N_i is the normalization fixed according to the observed CR data. Assuming the injected CR particles are produced in supernova remnants (SNR), the spatial distribution factor (f_S) should follow the SNR distribution and is given in cylindrical co-ordinates by,

$$f_S(r, z) = \left(\frac{r}{r_\odot}\right)^a \exp\left(-b.\frac{r - r_\odot}{r_\odot} - \frac{|z|}{z_s}\right). \tag{A4}$$

Here $r_\odot = 8.5\,$kpc is the Sun's distance from the galactic center, and $z_s = 0.2\,$kpc is the height of the galactic disk. $a = 1.25$ and $b = 3.56$ are fixed to reproduce the distribution of galactic CR sources based on Fermi-LAT γ-ray data, following the prescription in [116]. In our analysis the nuclear injection parameters in Eq. (A3) are set to their best-fit values derived by fitting to the latest AMS-02 proton data [119], and these values are shown in Tab. 3 for the MODA and MODB propagation profiles.

TABLE 3: Source parameters for profiles MODA, MODB based on [58] and [69] respectively.

Parameters	Model A	Model B
$R_{\rm br}$ (GV)	10	12.88
γ_p	2.336	1.79/2.45
$N_p\,(\mathrm{m^{-2}s^{-1}sr^{-1}GeV^{-1}})$	0.04783	0.0483

3. Galactic Magnetic Field

We introduced our choice of updated propagation profiles in Appendix A 1 that were obtained by fitting to the latest data of various secondary-to-primary ratios of nuclei in CRs. In the same spirit, we adopt a model for the Galactic Magnetic Field (GMF) [70] constrained by Faraday rotation measures from various experiments, and polarized synchrotron emission from the WMAP7 Galactic Synchrotron Emission map [120]. As discussed by the authors

of [70] in an earlier publication [37], the magnetic field in the halo has a different functional form than the field in the disk. Also, following [121, 122], they introduce a large-scale out-of-plane field and allow for striated random fields that contribute to the synchrotron emission. Their 21-parameter GMF model has also been incorporated in the latest versions of Galprop [123] and Dragon.

---

[1] O. Adriani et al. (PAMELA), Nature **458**, 607 (2009), 0810.4995.
[2] M. Ackermann et al. (Fermi-LAT), Phys. Rev. Lett. **108**, 011103 (2012), 1109.0521.
[3] O. Adriani et al. (PAMELA), Phys. Rev. Lett. **105**, 121101 (2010), 1007.0821.
[4] AMS-02 Collaboration, Talks at the AMS Days at CERN, 15-17 April 2015.
[5] L. Accardo et al. (AMS), Phys. Rev. Lett. **113**, 121101 (2014).
[6] M. Aguilar et al. (AMS), Phys. Rev. Lett. **113**, 121102 (2014).
[7] M. Aguilar et al. (AMS), Phys. Rev. Lett. **113**, 221102 (2014).
[8] D. Grasso et al. (Fermi-LAT), Astropart. Phys. **32**, 140 (2009), 0905.0636.
[9] J. Kopp, Phys. Rev. **D88**, 076013 (2013), 1304.1184.
[10] P. D. Serpico, Phys. Rev. **D79**, 021302 (2009), 0810.4846.
[11] D. Gaggero, L. Maccione, G. Di Bernardo, C. Evoli, and D. Grasso, Phys. Rev. Lett. **111**, 021102 (2013), 1304.6718.
[12] M. Di Mauro, F. Donato, N. Fornengo, R. Lineros, and A. Vittino, JCAP **1404**, 006 (2014), 1402.0321.
[13] I. Cholis and D. Hooper, Phys. Rev. **D88**, 023013 (2013), 1304.1840.
[14] M. Boudaud et al., Astron. Astrophys. **575**, A67 (2015), 1410.3799.
[15] D. Hooper, P. Blasi, and P. D. Serpico, JCAP **0901**, 025 (2009), 0810.1527.
[16] P. D. Serpico, Astropart. Phys. **39-40**, 2 (2012), 1108.4827.
[17] T. Linden and S. Profumo, Astrophys. J. **772**, 18 (2013), 1304.1791.
[18] E. W. Kolb and M. S. Turner, Front. Phys. **69**, 1 (1990).
[19] P. A. R. Ade et al. (Planck) (2015), 1502.01589.
[20] G. Steigman, B. Dasgupta, and J. F. Beacom, Phys. Rev. **D86**, 023506 (2012), 1204.3622.
[21] M. Kamionkowski and M. S. Turner, Phys. Rev. **D43**, 1774 (1991).
[22] M. Cirelli, M. Kadastik, M. Raidal, and A. Strumia, Nucl. Phys. **B813**, 1 (2009), [Addendum: Nucl. Phys.B873,530(2013)], 0809.2409.
[23] J. Hisano, S. Matsumoto, M. M. Nojiri, and O. Saito, Phys. Rev. **D71**, 063528 (2005), hep-ph/0412403.
[24] M. Cirelli, A. Strumia, and M. Tamburini, Nucl. Phys. **B787**, 152 (2007), 0706.4071.
[25] N. Arkani-Hamed, D. P. Finkbeiner, T. R. Slatyer, and N. Weiner, Phys. Rev. **D79**, 015014 (2009), 0810.0713.
[26] M. Pospelov, A. Ritz, and M. B. Voloshin, Phys. Lett. **B662**, 53 (2008), 0711.4866.
[27] D. Hooper, A. Stebbins, and K. M. Zurek, Phys. Rev. **D79**, 103513 (2009), 0812.3202.
[28] L. Pieri, J. Lavalle, G. Bertone, and E. Branchini, Phys. Rev. **D83**, 023518 (2011), 0908.0195.
[29] G. Bertone, M. Cirelli, A. Strumia, and M. Taoso, JCAP **0903**, 009 (2009), 0811.3744.
[30] M. Cirelli and M. Taoso (2016), 1604.06267.
[31] M. Cirelli, P. Panci, and P. D. Serpico, Nucl. Phys. **B840**, 284 (2010), 0912.0663.
[32] M. Ackermann et al. (Fermi-LAT), Astrophys. J. **761**, 91 (2012), 1205.6474.
[33] M. Ackermann et al. (Fermi-LAT), Phys. Rev. **D89**, 042001 (2014), 1310.0828.

[34] M. Ackermann et al. (Fermi-LAT), Phys. Rev. Lett. **115**, 231301 (2015), 1503.02641.
[35] F. Nesti and P. Salucci, JCAP **1307**, 016 (2013), 1304.5127.
[36] R. Beck, in American Institute of Physics Conference Series, edited by F. A. Aharonian, W. Hofmann, and F. M. Rieger (2011), vol. 1381 of American Institute of Physics Conference Series, pp. 117–136, 1104.3749.
[37] R. Jansson, G. R. Farrar, A. H. Waelkens, and T. A. Ensslin, JCAP **0907**, 021 (2009), 0905.2228.
[38] Y. Genolini, A. Putze, P. Salati, and P. D. Serpico, Astron. Astrophys. **580**, A9 (2015), 1504.03134.
[39] S. Galli, F. Iocco, G. Bertone, and A. Melchiorri, Phys. Rev. **D80**, 023505 (2009), 0905.0003.
[40] T. R. Slatyer, N. Padmanabhan, and D. P. Finkbeiner, Phys. Rev. **D80**, 043526 (2009), [arXiv:0906.1197 [astro-ph.CO]].
[41] R. Cen, Astrophys. J. **546**, L77 (2001), astro-ph/0005206.
[42] M. Abdelqader and F. Melia, Mon. Not. Roy. Astron. Soc. **388**, 1869 (2008), 0806.0602.
[43] F. J. Sanchez-Salcedo, Astrophys. J. **591**, L107 (2003), astro-ph/0305496.
[44] A. H. G. Peter, Phys. Rev. **D81**, 083511 (2010), 1001.3870.
[45] N. F. Bell, A. J. Galea, and K. Petraki, Phys. Rev. **D82**, 023514 (2010), 1004.1008.
[46] W. J. G. de Blok, Adv. Astron. **2010**, 789293 (2010), 0910.3538.
[47] A. A. Klypin, A. V. Kravtsov, O. Valenzuela, and F. Prada, Astrophys. J. **522**, 82 (1999), astro-ph/9901240.
[48] B. Moore, S. Ghigna, F. Governato, G. Lake, T. R. Quinn, J. Stadel, and P. Tozzi, Astrophys. J. **524**, L19 (1999), astro-ph/9907411.
[49] B. Moore, Nature **370**, 629 (1994).
[50] R. A. Flores and J. R. Primack, Astrophys. J. **427**, L1 (1994), astro-ph/9402004.
[51] P. Salucci and A. Burkert, Astrophys. J. **537**, L9 (2000), astro-ph/0004397.
[52] M. Boylan-Kolchin, J. S. Bullock, and M. Kaplinghat, Mon. Not. Roy. Astron. Soc. **415**, L40 (2011), 1103.0007.
[53] M. Aguilar et al. (AMS), Phys. Rev. Lett. **110**, 141102 (2013).
[54] M. Ackermann et al. (Fermi-LAT), Phys. Rev. **D82**, 092004 (2010), 1008.3999.
[55] O. Adriani et al. (PAMELA), Phys. Rev. Lett. **106**, 201101 (2011), 1103.2880.
[56] G. Giesen, M. Boudaud, Y. Gnolini, V. Poulin, M. Cirelli, P. Salati, and P. D. Serpico, JCAP **1509**, 023 (2015), 1504.04276.
[57] `https://github.com/grapes-dev/DRAGON/wiki`.
[58] S.-J. Lin, Q. Yuan, and X.-J. Bi, Phys. Rev. **D91**, 063508 (2015), 1409.6248.
[59] M. Mori, Astropart. Phys. **31**, 341 (2009), 0903.3260.
[60] M. Cirelli, G. Corcella, A. Hektor, G. Hutsi, M. Kadastik, P. Panci, M. Raidal, F. Sala, and A. Strumia, JCAP **1103**, 051 (2011), [Erratum: JCAP1210,E01(2012)], 1012.4515.
[61] P. Ciafaloni, D. Comelli, A. Riotto, F. Sala, A. Strumia, and A. Urbano, JCAP **1103**, 019 (2011), 1009.0224.
[62] J. F. Navarro, C. S. Frenk, and S. D. M. White, Astrophys. J. **490**, 493 (1997), astro-ph/9611107.
[63] J. Bovy and S. Tremaine, Astrophys. J. **756**, 89 (2012), 1205.4033.
[64] P. Salati, PoS **CARGESE2007**, 009 (2007).
[65] M. Cirelli, Pramana **79**, 1021 (2012), 1202.1454.
[66] AMS-02 Collaboration, presentation given at ICRC 2013, `http://www.ams02.org/2013/07/newresults-from-ams-presented-at-icrc-2013/`.

[67] D. Maurin, F. Donato, R. Taillet, and P. Salati, Astrophys. J. **555**, 585 (2001), astro-ph/0101231.
[68] D. Maurin, R. Taillet, and F. Donato, Astron. Astrophys. **394**, 1039 (2002), astro-ph/0206286.
[69] H.-B. Jin, Y.-L. Wu, and Y.-F. Zhou, JCAP **1509**, 049 (2015), 1410.0171.
[70] R. Jansson and G. R. Farrar, Astrophys. J. **757**, 14 (2012), 1204.3662.
[71] L. Fisk, **76**, 221 (1971).
[72] The value for the Fisk potential quoted in the text is obtained by taking the mean of the annual modulation values available at `http://cosmicrays.oulu.fi/phi/Phi_mon.txt` during the AMS-02 data taking period.
[73] S. Ting, PoS **ICRC2015** (2015), URL `http://pos.sissa.it/cgi-bin/reader/conf.cgi?confid=236`.
[74] E. Aliu et al. (VERITAS), Phys. Rev. **D85**, 062001 (2012), [Erratum: Phys. Rev.D91,no.12,129903(2015)], 1202.2144.
[75] A. Abramowski et al. (HESS), Phys. Rev. **D90**, 112012 (2014), 1410.2589.
[76] A. Lopez, C. Savage, D. Spolyar, and D. Q. Adams, JCAP **1603**, 033 (2016), 1501.01618.
[77] A. Scaffidi, K. Freese, J. Li, C. Savage, M. White, and A. G. Williams (2016), 1604.00744.
[78] P. Ullio and M. Valli (2016), 1603.07721.
[79] K. Hayashi, K. Ichikawa, S. Matsumoto, M. Ibe, M. N. Ishigaki, and H. Sugai (2016), 1603.08046.
[80] N. W. Evans, J. L. Sanders, and A. Geringer-Sameth (2016), 1604.05599.
[81] M. Papucci and A. Strumia, JCAP **1003**, 014 (2010), 0912.0742.
[82] T. R. Slatyer, Phys. Rev. **D93**, 023527 (2016), 1506.03811.
[83] `http://nebel.rc.fas.harvard.edu/epsilon/`.
[84] N. Padmanabhan and D. P. Finkbeiner, Phys. Rev. **D72**, 023508 (2005), astro-ph/0503486.
[85] H. Baer, K.-Y. Choi, J. E. Kim, and L. Roszkowski, Phys. Rept. **555**, 1 (2015), 1407.0017.
[86] T. R. Slatyer, Phys. Rev. **D87**, 123513 (2013), 1211.0283.
[87] T. R. Slatyer, Phys. Rev. **D93**, 023521 (2016), 1506.03812.
[88] V. Poulin, P. D. Serpico, and J. Lesgourgues, JCAP **1512**, 041 (2015), 1508.01370.
[89] Wolfram Research Inc., Mathematica 10.4 (2010), URL `http://www.wolfram.com`.
[90] D. P. Finkbeiner, S. Galli, T. Lin, and T. R. Slatyer, Phys. Rev. **D85**, 043522 (2012), 1109.6322.
[91] R. Diamanti, L. Lopez-Honorez, O. Mena, S. Palomares-Ruiz, and A. C. Vincent, JCAP **1402**, 017 (2014), 1308.2578.
[92] H. Liu, T. R. Slatyer, and J. Zavala (2016), 1604.02457.
[93] M.-Y. Wang, R. A. C. Croft, A. H. G. Peter, A. R. Zentner, and C. W. Purcell, Phys. Rev. **D88**, 123515 (2013), 1309.7354.
[94] S.-H. Oh, W. J. G. de Blok, E. Brinks, F. Walter, and R. C. Kennicutt, Jr, Astron. J. **141**, 193 (2011), 1011.0899.
[95] E. J. Tollerud, J. S. Bullock, L. E. Strigari, and B. Willman, Astrophys. J. **688**, 277 (2008), 0806.4381.
[96] J. S. Bullock, A. V. Kravtsov, and D. H. Weinberg, Astrophys. J. **539**, 517 (2000), astro-ph/0002214.
[97] A. J. Benson, C. S. Frenk, C. G. Lacey, C. M. Baugh, and S. Cole, Mon. Not. Roy. Astron. Soc. **333**, 177 (2002), astro-ph/0108218.
[98] F. Governato, A. Zolotov, A. Pontzen, C. Christensen, S. H. Oh, A. M. Brooks, T. Quinn,

S. Shen, and J. Wadsley, Mon. Not. Roy. Astron. Soc. **422**, 1231 (2012), 1202.0554.
[99] S. Garrison-Kimmel, M. Rocha, M. Boylan-Kolchin, J. Bullock, and J. Lally, Mon. Not. Roy. Astron. Soc. **433**, 3539 (2013), 1301.3137.
[100] D. H. Weinberg, J. S. Bullock, F. Governato, R. K. de Naray, and A. H. G. Peter (2013), 1306.0913, URL `https://inspirehep.net/record/1237028/files/arXiv:1306.0913.pdf`.
[101] M.-Y. Wang, A. H. G. Peter, L. E. Strigari, A. R. Zentner, B. Arant, S. Garrison-Kimmel, and M. Rocha, Mon. Not. Roy. Astron. Soc. **445**, 614 (2014), 1406.0527.
[102] L. Verde, P. Protopapas, and R. Jimenez, Phys. Dark Univ. **2**, 166 (2013), 1306.6766.
[103] R. A. Battye, T. Charnock, and A. Moss, Phys. Rev. **D91**, 103508 (2015), 1409.2769.
[104] G. Mangano, G. Miele, S. Pastor, T. Pinto, O. Pisanti, and P. D. Serpico, Nucl. Phys. **B729**, 221 (2005), hep-ph/0506164.
[105] A. G. Riess et al. (2016), 1604.01424.
[106] G. Mangano and P. D. Serpico, Physics Letters B **701**, 296 (2011), 1103.1261.
[107] J. Lesgourgues, G. Marques-Tavares, and M. Schmaltz, JCAP **1602**, 037 (2016), 1507.04351.
[108] M. Cirelli (2015), 1511.02031.
[109] J. C. Pober et al., Astrophys. J. **782**, 66 (2014), 1310.7031.
[110] A. Mesinger, A. Ferrara, B. Greig, I. Iliev, G. Mellema, J. Pritchard, and M. G. Santos (SKA EoR/CD Science Team), PoS **AASKA14**, 011 (2015), 1501.04106.
[111] J. Buch, M. Cirelli, G. Giesen, and M. Taoso, JCAP **1509**, 037 (2015), 1505.01049.
[112] `http://galprop.stanford.edu/`.
[113] G. Di Bernardo, C. Evoli, D. Gaggero, D. Grasso, and L. Maccione, JCAP **1303**, 036 (2013), 1210.4546.
[114] E. Orlando and A. Strong, Mon. Not. Roy. Astron. Soc. **436**, 2127 (2013), 1309.2947.
[115] A. Putze, L. Derome, and D. Maurin, Astron. Astrophys. **516**, A66 (2010), 1001.0551.
[116] R. Trotta, G. Johannesson, I. V. Moskalenko, T. A. Porter, R. R. de Austri, and A. W. Strong, Astrophys. J. **729**, 106 (2011), 1011.0037.
[117] V. S. Ptuskin and V. N. Zirakashvili, Astron. Astrophys. **403**, 1 (2003), astro-ph/0302053.
[118] T. Kamae, N. Karlsson, T. Mizuno, T. Abe, and T. Koi, Astrophys. J. **647**, 692 (2006), [Erratum: Astrophys. J.662,779(2007)], astro-ph/0605581.
[119] M. Aguilar et al. (AMS), Phys. Rev. Lett. **114**, 171103 (2015).
[120] B. Gold et al., Astrophys. J. Suppl. **192**, 15 (2011), 1001.4555.
[121] R. Beck, Magnetism in galaxies Observational overview and next generation radio telescopes, Advances in Plasma Astrophysics, Proceedings of the International Astronomical Union, `http://journals.cambridge.org/article_S1743921311007228`.
[122] T. R. Jaffe, J. P. Leahy, A. J. Banday, S. M. Leach, S. R. Lowe, and A. Wilkinson, Mon. Not. Roy. Astron. Soc. **401**, 1013 (2010), 0907.3994.
[123] A. W. Strong (2015), 1507.05020.